Characterization of hydroxyapatite: Before and after plasma spraying

EUNSUNG PARK[1], ROBERT A. CONDRATE[2] SR., DONGHUN LEE[2], KEITH KOCIBA[3], PATRICK K. GALLAGHER[3,4]
[1]*Medtronic AVE, St. Paul, MN 55113*
[2]*New York State College of Ceramics, Alfred University, Alfred NY 14802*
[3]*Department of Chemistry,* [4]*Department of Materials Science and Engineering, The Ohio State University, Columbus, OH 43210*

Hydroxyapatite (HA) powder was characterized before and after plasma spraying using infrared spectroscopy and thermoanalytical techniques. Structural changes were observed from the infrared spectra for the plasma-sprayed powder. These changes involved dehydroxylation and misoriented hydroxyl ions with different configurations. Dehydroxylation was accompanied by decreased intensities for the O-H stretching mode at 3571 cm^{-1} and the O-H librational mode at 633 cm^{-1}. A broad infrared band near 3400 cm^{-1} that was observed after spraying was attributed to the misoriented hydroxyl ions. The combined results from thermoanalytical techniques indicated that adsorbed water evolved in three stages below 500 °C, and that the dehydroxylation of HA started as low as 700 °C. A weight gain of the plasma sprayed HA was observed above 500 °C in inert atmospheres. This result indicates a strong tendency of dehydroxylated HA to restore hydroxyls. The decrease in the decomposition temperature of HA after spraying was attributed to largely perturbed structures.

1. Introduction

Hydroxyapatite (HA, $Ca_{10}(PO_4)_6(OH)_2$), has been a subject of extensive research for its use in hard tissue implantation due to its capability of promoting bone growth and bonding directly to bone. These advantages are based on the fact that HA has a structure closely resembling that of the primary inorganic phases of bones and teeth [1]. The use of HA, however, has been limited to non-load bearing applications because of its very low fracture toughness and poor resistance to fatigue failure [2] as compared to other implantable ceramics and metals. The application of HA as a coating on a metal implant first as a slurry [3] and then as a plasma sprayed coating [2] has been developed to use the advantages of both HA and titanium, (i.e. the bone bonding ability of HA, and the mechanical strength and toughness of titanium). Many studies have been conducted concerning plasma spray coating of HA [1, 4–7]. However, the characteristics of such coating are still not well defined.

Due to the rapid cooling of the HA particles during plasma spraying, the resultant coating does not adhere well to titanium. Such weakness at the interface between the HA coating and the titanium substrate was found to be due to the formation of amorphous calcium phosphate (CP) on rapid cooling [8]. In order to improve the interfacial bonding between HA and titanium, heat treatment of the coating is often necessary. Although such heat treatment enhances the interfacial bonding, how it affects the properties of HA coating has not been well investigated. Thorough understanding of the coating's thermal behavior is necessary.

There is also confusion concerning the comparison of results obtained by different investigators on the characteristics of HA coatings, such as impurity phases, crystallinity, solubility, long-term stability, etc. The properties of the coating are determined by many processing variables, including the plasma spray parameters as well as characteristics of the starting powders. Therefore, care should be taken when comparing the properties of coatings fabricated from different sources.

The purpose of this study was to define the characteristics and thermal behavior of the starting powders and plasma-sprayed coatings using X-ray powder diffraction (XRD), infrared (IR) spectroscopy and thermoanalytical techniques (TGA, DTA along with evolved gas analysis (EGA) utilizing mass spectrometry (MS)). Combining the results of these techniques facilitated correlation of the characteristics of HA before and after plasma spraying. Thermal events which occurred at high temperatures were also characterized in this manner.

2. Experimental procedure

2.1. Powder characteristics

Three HA powders (labeled as A, B and C) were used in this study. Particle size and the specific surface area of each powder were measured using a laser scattering

particle size analyzer and the multipoint BET gas adsorption method, respectively. The morphology of powders was studied using a scanning electron microscope.

The phase-purity with a resolution of 1% was determined with X-ray diffractometer involving a scan speed of 2.4°/min recording between 20 and 60° 2θ using Cu K_α radiation.

2.2. Plasma spraying

HA powder was plasma sprayed on stainless steel foils in order to reclaim the coating for analysis. A detailed description of the spraying conditions and parameters can be found in a previous study [8].

2.3. IR spectroscopy

IR transmission spectroscopy was used to study the powder characteristics that were not detectable by XRD, such as hydroxyl and carbonate contents. The spectra were obtained using a Nicolet 60 SXR FTIR spectrometer. The spectra were measured over the 4000–400 cm^{-1} region at 1 cm^{-1} resolution. Each spectrum was scanned 2048 times to increase the signal-to-noise ratio.

2.4. Thermal analysis

Three independent thermoanalytical techniques – thermogravimetric analysis (TGA), differential thermal analysis (DTA), and evolved gas analysis using mass spectrometry (EGA/MS) – were used to characterize the thermal behavior of the powder samples. Nearly identical experimental conditions were used for each technique (i.e. 20 mg of sample, 20 °C/min of heating rate and helium flowing at 40 ml/min). The reference crucible was always filled with 99.9% alumina powder very close to the mass of the sample powder. A Perkin-Elmer TGA 7 model was used for the TGA experiments in which the furnace had an upper temperature limit of 1000 °C. For the DTA measurements, the Perkin-Elmer DTA 7 model was also used, and the upper temperature limit of the DTA experiments was 1400 °C.

Evolved gas analysis over the range 60–1000 °C was performed using a quadrupole mass spectrometer (United Technologies, Inc.) evacuated by a turbomolecular pump. The mass range m/z 1–100 was recorded. The lower temperature limit was above the ambient temperature because the ionizing filaments acted as radiative heating elements when current was applied, thus raising the temperature of the system. The system pressure during the controled heating segment of these experiments was in the lower 10^{-6} torr range.

3. Results

3.1. Powder characteristics

The particle sizes and the specific surface areas were determined for powders A, B and C. The particle size of powder A ranged from 40 to 133 μm with a mean particle size of 64 μm and a specific surface area of 1.2 m^2/g. Powder B has wider size distribution (7–133 μm). The mean particle size is 59 μm, and the specific surface is 1.6 m^2/g. The powder C has the smallest mean particle size (8 μm) ranging from 0.15 to 35 μm and the largest specific surface area 72 m^2/g).

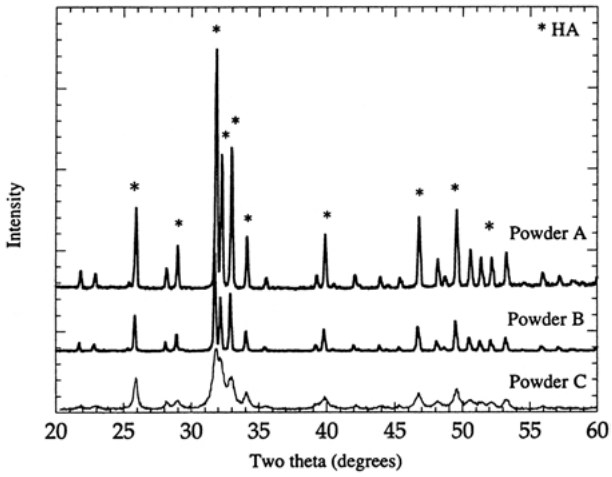

Figure 1 XRD patterns for the as-received HA powders A, B and C.

Scanning electron micrographs illustrate the morphology of three different powders. The particle shapes of both A and B powders are spherical, and appear to have a very similar morphology. High magnification micrographs of these powders revealed that individual particles are composed of fine primary particles (< 1 μm). However, the particles in powder B have rougher surfaces. The particles in powder C have irregular shapes and the roughest surfaces.

Fig. 1 shows the XRD patterns for the three starting powders. Powders A and B appear to be highly crystalline, exhibiting well-defined sharp diffraction peaks. Powder C also exhibits peaks corresponding to HA; however, all peaks are broader. Although peaks at 31 and 32.5° 2θ are indicative of the presence of β-tricalcium phosphate (TCP) phases, the absence of other peaks at 34.4 and 29.8° 2θ indicates that powder C does not contain a detectable amount of β-TCP.

After spraying the powder A using Ar/H_2 gas, the XRD pattern exhibits diffraction peaks equivalent to those of the starting powder, but slightly broader (see

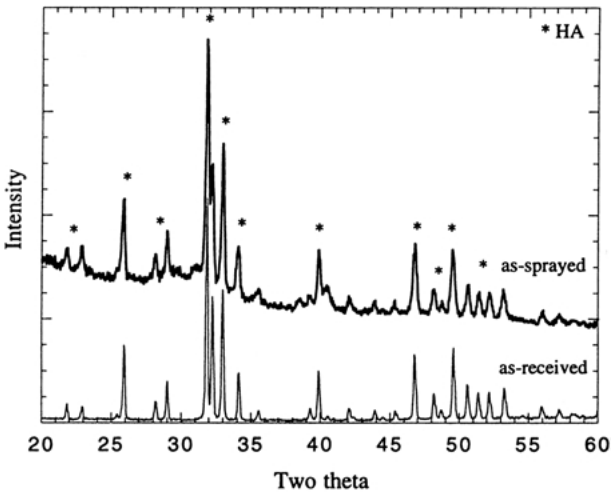

Figure 2 XRD pattern for HA powder A before and after plasms spraying.

Fig. 2). Possible reasons for peak broadening are smaller crystal size, stresses in the material, and the absence of long-range order.

3.2. IR spectroscopy

The IR spectra of the as-received and sprayed powder are shown in Fig. 3. The two strong bands found at 602 and 571 cm^{-1} are two factor-group split components of the asymmetric O-P-O bending mode (ν_4). The weak bands that appeared at 473 and 436 cm^{-1} are attributed to the symmetric O-P-O bending mode (ν_2). The very strong but broad band at 1045 cm^{-1} and a medium sharp band at 1090 cm^{-1} are assigned to factor-group split components of the asymmetric P-O stretching mode (ν_3). A weak shoulder at 1070 cm^{-1} appears to be the third component of the ν_3 band. The non-degenerate symmetric P-O stretching mode (ν_1) is observed as the small sharp band at 960 cm^{-1}.

The strong band at 3571 cm^{-1} can be unambiguously assigned to the lattice OH stretching vibration [9]. The band at 632 cm^{-1} is due to the OH librational mode [10]. The weak broad band at 1470 cm^{-1} and the very weak band at 1417 cm^{-1} are attributed to the stretching vibration of carbonates. Although both bands are due to carbonates, they originate from different molecular configurations for the carbonate ions. Carbonates in the aragonite structure appear to produce an absorption band at 1470 cm^{-1}, while free carbonate exhibits a band at 1415 cm^{-1} [11]. The band assignments for PO_4^{3-} and OH^- ions in both as-received and plasma sprayed HA are listed in Table I.

3.3. Thermal anlaysis

The combined results from TGA, DTA and EGA/MS for the as-received and plasma-sprayed powder A are shown in Figs 4 and 5. The magnitude of the total ion current (TIC) peaks and the temperatures of the weight losses in the TGA results correlate very well as shown in Fig. 4.

TABLE I IR band assignments for PO_4^{3-} and OH^- groups in HA before and after plasma spraying (powder A)

Band	Before	After
ν_1	960	sh*
ν_2	473	473
	436	438
ν_3	1090	1090
	1070	1050
	1045	new band at 990
ν_4	602	602
	571	571
		new band at 550
$\nu_{S,OH}$	3571	3571
		new bands at 3641, 3437
$\nu_{1,OH}$	632	sh
$2\nu_2$ overtones,	2149	2144
combination bands	2077	2077
	1994	2000

*sh: Band disappeared leaving very weak shoulder.

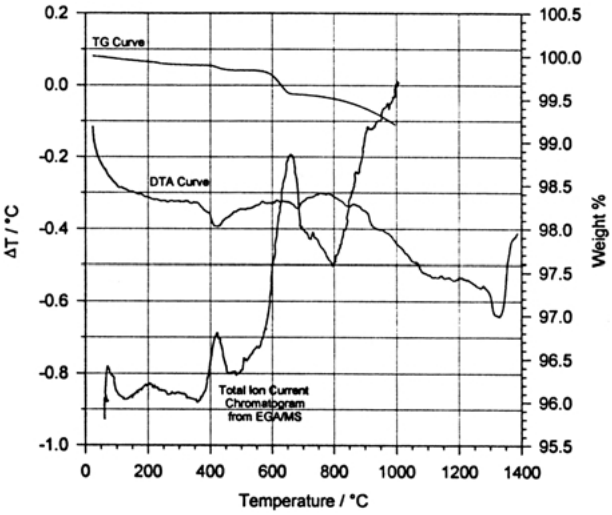

Figure 4 TGA, DTA and EGA/MS results for the HA powder A.

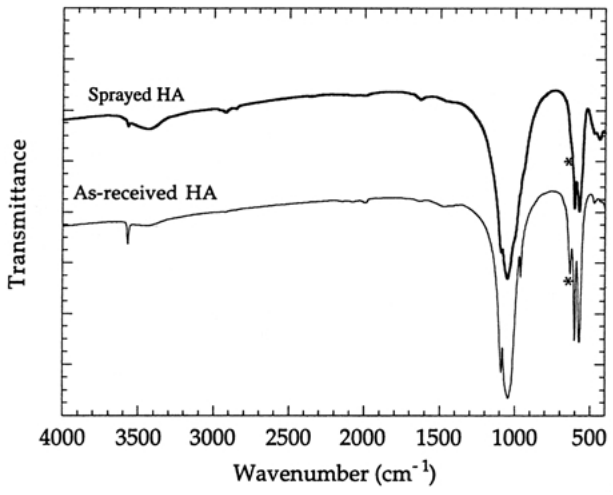

Figure 3 IR spectra for HA powder A before and after plasma spraying. (Asterisks indicate the disappearence of the O-H librational band after spraying.)

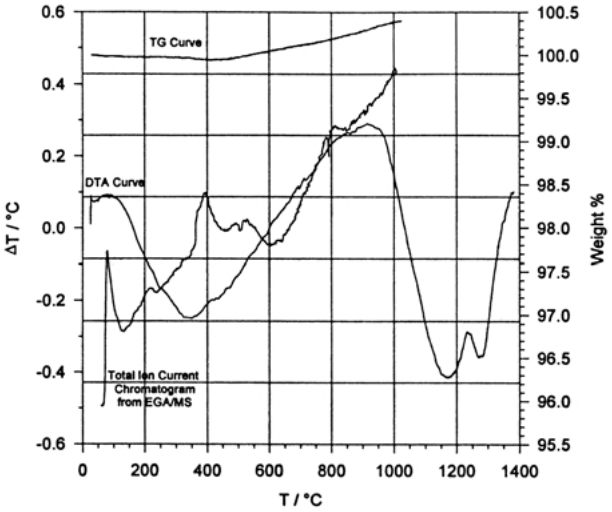

Figure 5 TGA, DTA and EGA/MS results for the plasma sprayed HA powder A.

4. Discussion

4.1. Powder selection

For plasma spraying, starting powders should be selected by controlling the powder variables such as particle size and distribution, particle shape and composition (or purity). Large particles are preferred in order to obtain a highly crystalline coating [1, 12] because small particles are completely melted during plasma spraying. Inordinately large particles, however, often produce unmelted particles and consequently rough coating surfaces [13]. The particle size distribution should therefore be narrow to avoid both of these difficulties and to help ensure that the particles melt uniformly. Particle shape is also important since the angular particles do not readily flow during spraying; this often results in a blocked powder feed hose and highly porous coatings [12].

According to ASTM specification F-1185-88 [14], HA coating should contain a minimum of 95% HA in order to be used for surgical implants. In order to retain more than 95% HA after plasma spraying, the starting powder has to be very pure and 100% crystalline because plasma spraying produces impurity phases such as β-TCP, tetracalcium phosphate (TeCP), CaO, and amorphous calcium phosphate (CP).

By considering the aforementioned powder variables, the powders A and B were used throughout this study. This is based on combining the results from particle size, SEM and XRD measurement which showed that powders A and B have large enough particle sizes to be sprayed, and that their particles are spherical in shape, and highly crystalline with no impurity phases. Between the two powders, powder A was specifically chosen for plasma spraying because powder A was made fresh. Powder C was discarded due to its small particle size, angular particle shape and impurity phases, such as amorphous CP phases and β-TCP.

4.2. IR spectral study of HA

The band assignments for the as-received HA (as discussed previously) are consistent with those made by Blakeslee and Condrate [15]. Additional observed bands are the weak bands in the 2000 cm^{-1} region (2149, 2077, 1994 cm^{-1}) which are assigned to $2\nu_3$ overtones and a combination band of ν_1 and ν_3 based on the observation made by Baddiel and Berry [16].

Plasma spraying caused some structural changes in HA. First, the relative intensity of the band at 3571 cm^{-1} due to the OH stretching vibration decreased by 75% (see Fig. 6). This undoubtedly indicates the loss of hydroxyls during spraying. This is also supported by the disappearance of the OH libration band at 632 cm^{-1} as indicated in Fig. 3. The broad band near 3400 cm^{-1} became broader and more intense. This band is often accompanied by a water deformation band at 1630 cm^{-1}, and can be attributed to adsorbed water [17, 18]. Some species other than adsorbed water have also been suggested to contribute to this absorption by Cant *et al*. [17]. The idea of possible contribution to an absorption band from species other than adsorbed water is also supported by the increased intensity of the band at 1630 cm^{-1} from the sprayed HA because no reason was found to believe that plasma-sprayed coatings should adsorb more water than the as-received HA powder.

If this band is due to hydroxyl ions, the low wavenumber can be regarded as evidence of hydrogen bonding. Two mechanisms were suggested through which hydrogen bonding can operate [16]. The first mechanism involves a decreased distance between the hydroxyl ions and the phosphate oxygens nearby, (i.e. OH-OPO_3 type). The distance was estimated to be 3.068 Å [16]. The empirical relationship between OH-O and OH stretching vibration wavenumber was suggested by Nakamoto *et al*. [19], from which a stretching wavenumber of 3630 cm^{-1} is predicted for a distance of 3.068 Å. This wavenumber is, however, too high compared with the observed wavenumber of 3437 cm^{-1}, although Nakamoto's relationship assumes a linear OH-O arrangement. The second possible mechanism for hydrogen bonding is by the interactions between neighboring hydroxyl ions. Cant *et al*. [17] suggested a different hydroxyl ion position inside the HA structure (see Fig. 7). The hydroxyl ions can straddle across the Ca triangles lying on the mirror plane. This arrangement reduces the OH-O distance between neighboring hydroxyl groups to 2.84 Å [17], which predicts an OH stretching frequency of 3430 cm^{-1} on the basis of Nakamoto's relationship. This is very close to the observed wavenumber of 3437 cm^{-1}. The idea of having misoriented hydroxyl ions is further supported by the nature of plasma spraying. Plasma spray produces highly perturbed structures, because it involves high temperature and high velocity impact. The broadness of the band is presumably due to the distribution of the hydroxyl ions located in non-equivalent sites having different interatomic distances.

The small band appearing at 3641 cm^{-1} can be attributed to $Ca(OH)_2$, which also produces an absorption band at 3544 cm^{-1} [20]. The appearance of this band might imply that CaO has formed during plasma spraying and transformed to $Ca(OH)_2$ on cooling in air.

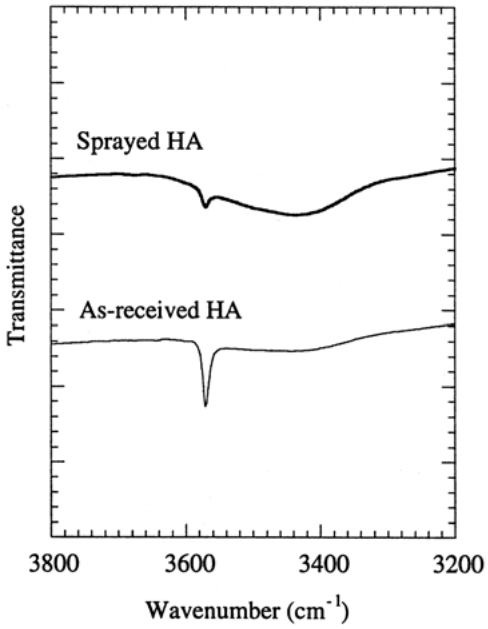

Figure 6 IR spectra of the HA powder A before and after plasma spraying, showing the OH stretching vibration band 3571 cm^{-1}.

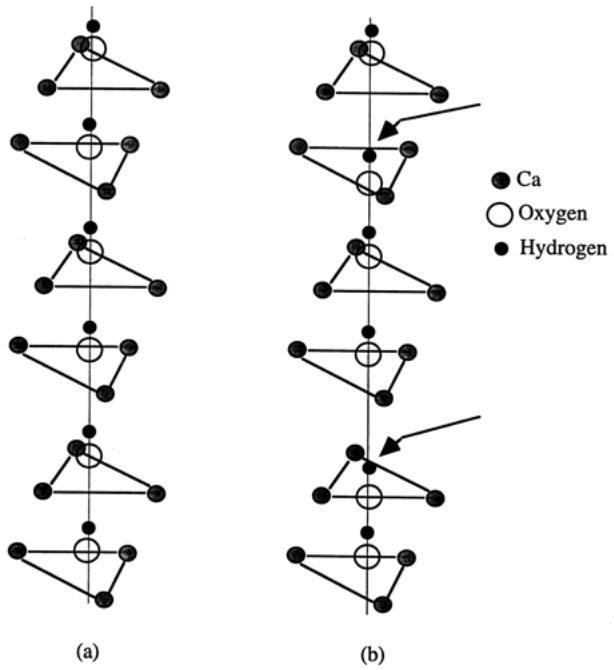

Figure 7 Possible arrangements of hydroxyl ions in hydroxyapatites: (a) ordered structure and (b) structure with misoriented hydroxyl ions. The arrows indicate straddled hydroxyl ions. (Adapted from Cant *et al.* [17].)

However, lack of XRD peaks corresponding to CaO or $Ca(OH)_2$ seems to exclude the possibility of the formation of a large amount under the spraying conditions used in this experiment. An alternative explanation is that the hydroxyl ions are located in a similar molecular configuration as the $Ca(OH)_2$ in a way that the hydroxyl columns are terminated by the crystal surfaces.

Other changes observed after spraying include the loss of the symmetric stretching mode for phosphate at $960\,cm^{-1}$ and new shoulders appearing at 990, 942 and $550\,cm^{-1}$. The loss of the symmetric stretching mode at $960\,cm^{-1}$ indicates that the environment around phosphate ions had changed after spraying in such a way that the symmetry of phosphate ions was lowered. The band at $942\,cm^{-1}$ can be attributed to β-TCP because β-TCP exhibits an asymmetric P-O stretching mode at $945\,cm^{-1}$ [21]. This is, however, not convincing since other bands corresponding to β-TCP are missing. Furthermore, XRD results showed only a trace amount of β-TCP formed. It is interesting that shoulders at 990 (ν_3), 945 (ν_1) and 550 (ν_4) were observed with partial substitution of oxygen with ^{18}O [9]. Radin and Duchyene [4] also observed these bands, and attributed them to the characteristic bands of ''oxy-hydroxyapatite''. However, oxy-hydroxyapatite is not well defined, and its presence is still controversial. Further explanation requires systematic studies.

4.3. Thermal behavior of HA

The EGA/MS results for the as-received powder A shows water evolution at 90 200 and 420 °C (see Fig. 8). The water evolution near 90 °C probably originates from water adsorbed to powder surfaces. The evolution at 200 °C may be from water trapped inside pores as reported by Helga *et al*. [22]. This peak is absent from the EGA/MS results for powder B probably because powder A is more porous. At 420 °C, a weight loss due to water evolution is accompanied by an endothermic event observed in the DTA results which can be attributed to tightly bound water. Jamal and Khattech [23] observed a similar thermal event near 400 °C in a decomposition study of enamel. They, however, attributed it to the reaction between hydrogen phosphates and carbonates since CO_2 evolution was also observed at that temperature. They suggested the following reaction:

$$2HPO_4^{2-} + CO_3^{2-} = 2PO_4^{3-} + CO_2 + H_2O \qquad (1)$$

In fact, the EGA/MS results for carbon oxide series (see Fig. 9) shows small humps for carbon dioxide (m/z 44) and their molecular fragments (i.e. m/z 28 (CO), 16 (O) and 12 (C)) which supports the above-mentioned reaction. However, the high relative intensity (three times higher) of the water series compared with the carbon dioxides seems to indicate that the evolution of tightly bound water also contributes to this event. Furthermore, the infrared spectra showed no positive evidence of hydrogen phosphates before and after spraying.

Between 600 and 700 °C, species corresponding to carbon dioxide are evolved (see Fig. 9). Some loss may be due to carbon dioxide adsorbed to the powder surfaces or the equipment but the accompanied large weight loss seems to indicate that it was due primarily to the decomposition of carbonates. Fig. 4 shows a small endothermic peak at 680 °C. This peak is considered to be due to the decomposition of carbonates, and corresponds to an EGA/MS TIC peak at 640 °C. The difference of 40 °C originates from a downward shift of the reaction equilibrium temperatures in the EGA/MS

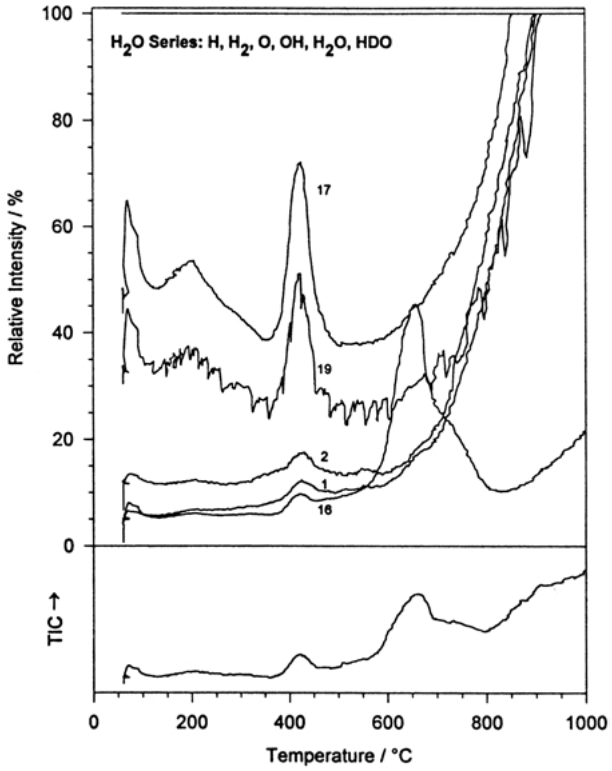

Figure 8 EGA/MS results for the as-received HA powder A, showing m/z values related to the water series.

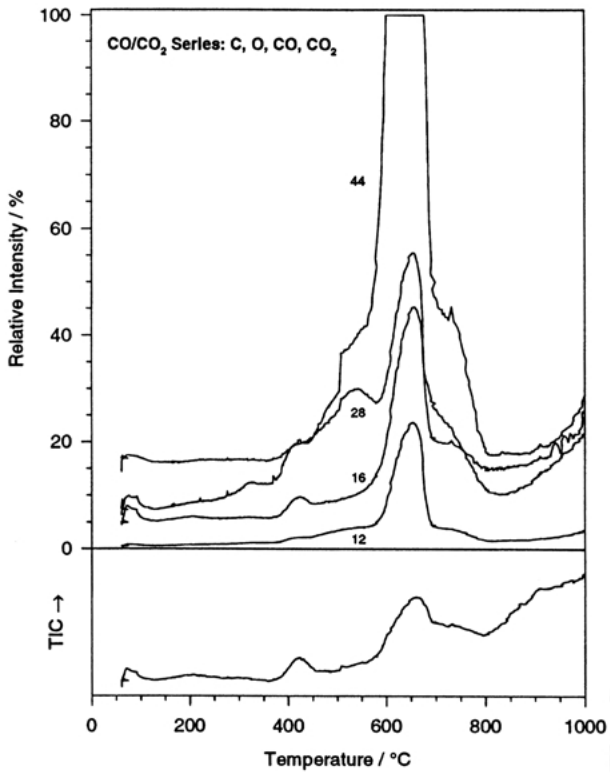

Figure 9 EGA/MS results for the as-received HA powder A, showing m/z values related to the carbon oxide series.

results that is caused by the reduced pressure environment of the sample relative to the DTA results. Carbonates are not necessarily present in the crystals originally but can be easily introduced during powder storage and handling. The IR spectra show small bands that appeared at 1470 and 1417 cm^{-1} which correspond to aragonite-type and free carbonates, respectively [11].

The EGA/MS results (see Fig. 8) indicate that OH-evolution rapidly increases to the saturation point above 700 °C with no other species evolved. The TGA results also indicate a continuous weight loss at temperatures above 700 °C up to 1000 °C. These results indicate that dehydroxylation of HA starts as low as 700 °C. This temperature is low compared with the reported temperature that is observed by IR spectroscopy in air (900 °C) [24]. The temperature difference between the two characterization techniques may be due to the vacuum environment and the sensitivity of the EGA/MS technique. In the IR spectra, the loss of OH^- is indicated by the decreased intensity of the OH stretching mode at 3571 cm^{-1} and the loss of the OH librational mode at 630 cm^{-1} as is shown in Fig. 3.

The total weight loss due to dehydroxylation between 700 and 1000 °C was estimated to be 0.34%, which is equivalent to the 10% loss of the total hydroxyl ions in HA since the hydroxyl ions are 3.4% of the total mass of stoichiometric HA. It has been suggested that up to 75% of water may be lost while retaining the HA structure [25]. One study showed that no structural changes were noted even after prolonged heating over 72 h at 1000 °C in air, while structural changes were indicated after heating in vacuum at 850 °C for 3 h [26]. The dehydroxylation can be expressed as the following relation [25]:

$$Ca_{10}(PO_4)_6(OH)_2 = Ca_{10}(PO_4)_6(OH)_{2-2x}O_x(\,)_x + xH_2O; x \geq 0.75 \quad (2)$$

where ( ) indicates vacancy.

The rapid rise shown in the TIC peak above 800 °C is due to the overall increase in the ion counts from H_2O, OH, H_2, H, CO_2 and CO gases. In this temperature range, EGA/MS analysis is very difficult and often inconclusive due to significant increases in background gas concentration.

An endothermic event at 1330 °C is an indication of the decomposition of HA by the following reaction:

$$Ca_{10}(PO_4)_6(OH)_2 \rightarrow 2Ca_3(PO_4)_2 + Ca_4P_2O_9 + H_2O \quad (3)$$

as was also observed by others [27]. The decomposition temperature depends on the partial pressure of water. For example, HA is stable up to 1400 °C in air [28] or decomposes at 1550 °C at $P(H_2O) = 500$ mmHg [29]. Arends *et al*. [30] suggested that HA decomposes to TCP and CaO instead of TCP and TeCP. However, unless the starting powder already contains CaO as an impurity, the coexistence of TCP and CaO without TeCP is very unlikely, if not impossible, because they coexist only within a limited composition range (Ca-rich region) at a single temperature under a fixed $P(H_2O)$ (see Fig. 10). Furthermore, if the HA structure can tolerate Ca-deficiency to compensate dehydroxylation [31], CaO does not form. In this case, β-TCP coexists with HA until HA decomposes to α-TCP and TeCP.

The thermal behavior for plasma-sprayed HA was found to be very similar to that observed for the as-received powder at least below 500 °C. A major gas evolution near 90 °C and a minor one at 200 °C were attributed to water. The sources of water can be the powder surfaces and pores as in the case of the as-

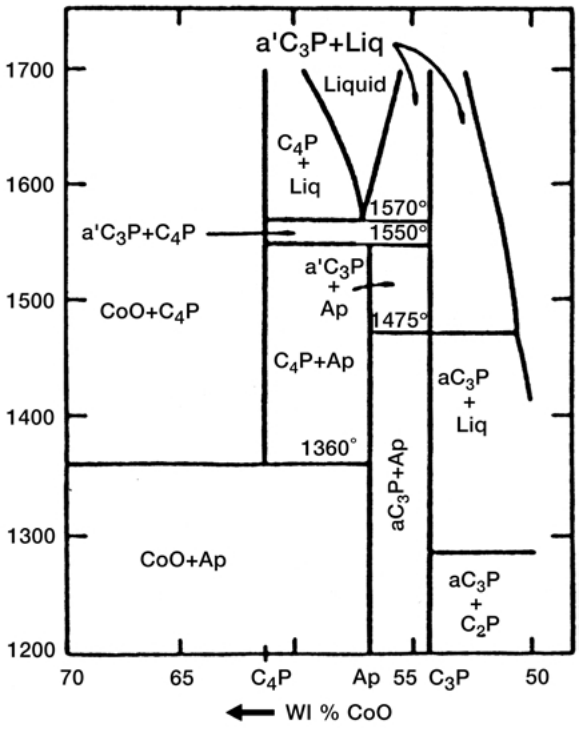

Figure 10 Phase diagram of the CaO-P_2O_5 system with $P(H_2O) = 500$ mm Hg [1].

received HA powder. The evolution at 400 °C appears to be related to water and CO_2 evolution.

The most confusing part of the thermal analysis of plasma-sprayed powder was the interpretation of the TGA results. The plasma-sprayed HA exhibited a gradual but continuous weight gain at temperatures above 500 °C, contrary to expectations considering that the atmosphere was inert (He). The amount of weight gain was small (0.4%); however, it was more than for the blank run (0.1%). The TGA run in air exhibited a weight gain above 500 °C which was three times larger than under the inert gases. This result is not surprising because plasma-sprayed HA is dehydroxylated, and it tends to rehydroxylate on heating in air [4].

In order to find the cause of the weight gain, the TGA was repeated first in nitrogen and then in argon using different instrumentation (SETARAM at Alfred). However, all results showed the same trend. In fact, this observation is consistent with that made by Trombe [25]. Dehydroxylated HA was shown to be very reactive, absorbing H_2O at approximately 600 °C even in a vacuum of 10^{-4} torr. A similar trend was also found by other groups using Ar [32] or He [33], although the amount of weight gain was different. Since similar trends were observed regardless of gas compositions or instrumentation, it is presumed that the weight gain under the inert atmosphere is due to water trapped inside the thermal analysis equipment. Whatever the source is, however, this clearly indicates that the plasma-sprayed HA has a strong tendency to recover the lost hydroxyls even in rigidly controlled conditions.

A difference observed between the powders before and after spraying is the absence of carbonate decomposition near 650 °C (see Fig. 5). The EGA/MS results, however, indicates that carbonate species evolved near 550 °C, which is 100 °C lower than the as-received powder. Moreover, the relative intensity of carbonates decreased more than 50%. This result implies that most of the carbonate ions that are present in HA are lost during spraying, and that the remaining ones are more loosely bound to the structure, possibly adsorbed to the powder surfaces. The IR spectra also indicated the loss of carbonate after spraying by decreased intensity of the band at 1470 cm^{-1}.

Another observed change due to spraying is the extremely broad deviation of the DTA curve from $\Delta T = 0$ °C, starting from 300 to 1100 °C. In this temperature range, the results seem to show a broad exothermic event. A similar trend has been observed for the plasma-sprayed HA over the temperature range between 400 and 700 °C [6] and was attributed to recrystallization of the amorphous phase. The exotherm observed in this study, however, seems to be too broad to be ascribed to recrystallization, although the onset temperature is very close to that which Vogel *et al.* [34] observed. They found that crystallization started as low as 300 °C. Although it is possible that such a broad exotherm is due to a kinetically hindered event, the heat capacity difference may also have caused it. It can also be attributed to the heat capacity difference between the plasma-sprayed HA and the Al_2O_3 used for the reference sample. The heat capacity of dense Al_2O_3 at room temperature is 1.12 J/g K [35]. Although heat capacity of plasma sprayed HA is not known, it will be close to that of a dehydroxylated HA which is 0.73 J/g K [24]. The DTA was repeated with similar results.

At 1270 °C, the DTA exhibited an endothermic peak which can be attributed to the decomposition of HA (see Fig. 5). This temperature is approximately 50 °C lower than that observed for the as-received HA (see Fig. 4). The decreased decomposition temperatures is believed to be due to the effect of plasma spray in that the HA is highly dehydroxylated and perturbed. Trombe [25] also observed that the dehydroxylated HA decomposed to a mixture of TCP and TeCP near 1050 °C. The temperature difference between two studies might be from the different degree of dehydroxylation and the partial pressure of water.

5. Conclusions

The as-received and the plasma-sprayed HA were characterized using XRD, SEM and IR spectroscopy along with three independent thermoanalytical techniques (TGA, DTA and EGA using mass spectrometry). Structural changes after plasma spraying were detected by IR spectroscopy and thermal analysis. Dehydroxylation was noted by the decreased intensity of the OH stretching vibration band at 3571 cm^{-1} and the loss of OH librational band at 630 cm^{-1}. A broad IR band near 3400 cm^{-1} observed after spraying was attributed to misoriented hydroxyl ions with different configurations. The combined results from different thermoanalytical techniques indicate that water evolved in three stages below 500 °C. These temperatures are not affected by plasma spraying. Thermal analysis also showed that dehydroxylation of HA started as low as 700 °C. Apparent weight gain of the plasma-sprayed HA above 500 °C was observed in inert atmospheres, regardless of gas compositions. This result indicates a strong tendency for dehydroxylated HA to restore hydroxyls that are lost during plasma spraying into the oxy-hydroxyapatite structure. Decomposition of the as-received HA occurred at 1330 °C. This temperature, however, decreased by 50 °C after spraying possibly due to largely perturbed structures.

References

1. C. P. A. T. KLEIN, J. G. C. WOLKE and K. DE GROOT, in ''An Introduction to Bioceramics'', edited by L. L. Hench and J. Wilson (World Scientific, Singapore, 1993) p. 199.
2. K. DE GROOT, R. GEESINK, C. P. A. T. KLEIN and P. SEREKIAN, *J. Biomed. Mater. Res.* **21** (1987) 1375–1381.
3. P. DUCHEYNE, L. L. HENCH and A. KAGAN, *ibid.* **14** (1980) 225.
4. S. R. RADIN and P. DUCHYENE, *J. Mater. Sci.: Mater. Med.* **3** (1992) 33–42.
5. W. R. LACEFIELD, in ''An Introduction to Bioceramics'', edited by L. L. Hench and J. Wilson (World Scientific, Singapore, 1993) p. 223.
6. R. MCPHERSON, N. GANE and T. J. BASTOW, *J. Mater. Sci.: Mater. Med.* **6**, (1995) 327–334.
7. C. Y. YANG, B. C. WANG, E. CHANG and J. D. WU, *ibid.* **6** (1995) 249–257.
8. E. PARK, D. T. HOELZER and R. A. CONDRATE, SR., *MRS Symp. Proc.* **458** (1997) 409–414.
9. B. O. FOWLER, *Inorg. Chem.* **13** (1974) 194–207.

10. B. O. FOWLER, E. C. MORENO and W. E. BROWN, *Arch. Oral Biol.* **11**(5) (1966) 477–492.
11. J. C. FARMER, ''Infrared spectra for minerals'', Mineralogical Society, London, (1974).
12. P. CHEANG and K. A. KHOR, *J. Therm. Spray Technol.* **5** (1996) 310–316.
13. K. A. KHOR and P. CHEANG, *ibid.* **3** (1994) 45–50.
14. ASTM designation: F1185–88, ''Standard specification for composition of ceramic hydroxylapatite for surgical implants''
15. K. C. BLAKESLEE and R. A. CONDRATE, SR., *J. Am. Ceram. Soc.* **54** (1971) 559–563.
16. C. B. BADDIEL and E. E. BERRY, *Spectrochim. Acta.* **22** (1966) 1407–1416.
17. N. W. CANT, J. A. S. BETT, G. R. WILSON and W. K. HALL, *ibid.* **27A** (1971) 425–439.
18. B. O. FOWLER, *ibid.* 207–214.
19. K. NAKAMOTO, M. MARGOSHES and R. E. RUNDLE, *J. Am. Chem. Soc.* **77** (1955) 6480.
20. W. R. BUSING and H. W. MORGAN, *J. Chem. Phys.* **28** (1958) 998.
21. A. SLOSARCZYK, C. PALUSZKIEWICZ, M. GAWLICKI and Z. PASZKIEWICZ, *Ceram. Int.* **23** (1997) 297–304.
22. H. FÜREDI-MILHOFER, V. HLADY, F. S. BAKER, R. A. BEEBE and N. W. WIKHOLM, *J. Colloid Interface Sci.* **70** (1979) 1–9.
23. M. JAMAL and I. KHATTECH, *Thermochim. Acta* **152** (1989) 65–76.
24. T. KIJIMA and M. TSUTSUMI, *J. Am. Ceram. Soc.* **62** (1979) 455–460.
25. J. C. TROMBE and G. MONTEL, *J. Inorg. Nucl. Chem.* **40** (1978) 15–21.
26. H. C. W. SKINNER, J. S. KITTELBERGER and R. A. BEEBE, *J. Phy. Chem.* **79** (1975) 2017–2019.
27. W. VAN RAEMDONCK, P. DUCHEYNE and P. DE MEESTER, in ''Metal and Ceramic Biomaterials'', Vol. 2, edited by P. Ducheyne and W. Hasting (CRC Press, Boca Raton, Florida, 1984) p. 149.
28. J. ZHOU, X. ZHANG, J. CHEN, S. ZENG and K. DE GROOT, *J. Mater. Sic. Mater. Med.* **4** (1993) 83–85.
29. P. V. RIBOUD, *Ann. Chim.* **8** (1973) 381.
30. J. ARENDS, J. CHRISTOFFERSEN, M. R. CHRISTOFFERSEN, H. ECKERT, B. O. FOWLER, J. C. HEUGHEBAERT, G. H. NANCOLLAS, J. P. YESINOWSKI and S. J. ZAWACKI, *J. Non Cryst.* **84** (1987) 515–532.
31. A. S. POSNER, J. M. STUTMAN and E. R. LIPPINCOTT, *Nature* **188** (1960) 486–487.
32. S. GARY, FISCHMAN. Private communication.
33. K. A. GROSS, ''The amorphous phases in hydroxyapatite coatings,'' Ph.D. Thesis, SUNY at Stony Brook, 1995.
34. J. VOGEL, C. RUSSEL, G. GUNTHER, P. HARTMANN, F. VIZETHUM and N. BERGNER, *J. Mater. Sci. Mater. Med.* **7** (1996) 495–499.
35. Ceramics and Glasses, Engineered materials handbook, Vol. 4, (ASM International, Columbus, OH, 1991) p. 752.

Received 19 April 2000
and accepted 27 February 2001